Trends in the Adsorption of Oxygen and Li_2O_2 on Transition-metal Carbide Surfaces: A Theoretical Study

Polina Tereshchuk,[†] Diana Golodnitsky,[‡] and Amir Natan*[,†,¶]

†*Department of Physical Electronics, Tel Aviv University, Israel 69978*
‡*School of Chemistry, Tel Aviv University, Israel*
¶*The Sackler Center for Computational Molecular and Materials Science, Tel-Aviv University, Tel-Aviv 69978, Israel*

E-mail: amirnatan@post.tau.ac.il

Abstract

In this work we performed fundamental investigations of the adsorption of O_2 and Li_2O_2 molecules on seven transition-metal carbide (TMC) surfaces, which present $3d$, $4d$ and $5d$ TM, where TM = Ti, V, Zr, Nb, Mo, Hf and Ta. We employed density functional theory (DFT) with the semilocal meta-GGA SCAN functional. The oxide layer behaves as a passivation layer on the TiC(111), ZrC(111) and MoC(001) systems upon Li_2O_2 adsorption, but promotes the formation of the $Li_1O_3TM_1$ layer on the VC(111), NbC(111), MoC(111), and HfC(111) surfaces due to the change in stoichiometry which is caused by the first adsorbed Li_2O_2 molecule. We showed that with increasing the number of the Li_2O_2 molecules on the TMC surfaces, the contribution of the TMC surface states turns out less important to the adsorption energy of the molecules. After the first layer of Li_2O_2 it approaches the native crystal values, which occurs faster with the occupation of the TM d-bands. This work can make a contribution in fundamental understanding and development of new, TMC-based, catalysts for alkali-metal batteries.

Introduction

Rechargeable Li$-O_2$ batteries have attracted great interest due to their excellent theoretical specific energy (11700 Wh/kg), which is about 5 times higher than that of conventional Li-ion batteries. In Li$-O_2$ batteries, the chemical reaction occurs between lithium as the anode material and air oxygen, and leads to the formation (discharge, the oxygen reduction reaction, ORR) and decomposition (charging, the oxygen evolution reaction, OER) of Li_2O_2, that is $2Li^+ + O_2 + 2e^- \rightleftharpoons Li_2O_2$.[1–4]

The air cathode takes an active part in the performance of Li$-O_2$ batteries, in particular it affects Coulombic efficiency, charge/discharge overpotential and power capability. A good cathode catalyst should be able to facilitate both ORR and OER, especially OER, because of higher energetic barriers, which result in slow OER kinetics.[5] Thus, design of suitable cathode materials for Li$-O_2$ batteries is a great challenge.

A number of catalytic materials have been suggested recently in the literature.[2,3,5] Initially, porous carbon was proposed as a promising cathode material for Li$-O_2$ batteries.[1] However, it is found to be unstable at the Li_2O_2 oxidation stage.[6] Other catalysts which were proposed in literature are: modified carbon, metals, metal alloys, oxides, and others (see reviews[2,3,5] and citations therein).

Among the perspective catalytic materials, it is worth to point out transition-metal carbides (TMC). Recent experimental studies suggested TiC[7,8] and Mo_2C[9] based catalysts as having a great potential as cathode materials for Li$-O_2$ batteries, Faktorovich-Simon et al.[10] have also evaluated TiC as a cathode material for Na$-O_2$ batteries. For example, TiC cathode, with electrolyte based on dimethyl sulphoxide, yields excellent reversibility of the formation/decomposition of Li_2O_2 (> 98% capacity retention after 100 cycles). Moreover, TiC catalyst was found to weaken side reactions originating from the degradation of electrolyte and electrode at Li_2O_2 deposition.[7] It is found to be stable due to the formation of TiO_2 (and some TiOC) surface layers[7] or other protective surface layers containing elemental carbon, oxides and oxycarbides on the oxidized TiC surface.[8] Hence, theoretical investigations of the interaction of Li_2O_2 with TMC surfaces can be useful for the design of new catalysts.

The adsorption of Li_2O_2 on TiC surfaces was theoretically investigated by several works.[11–14] In a previous work[13] we have also analyzed the adsorption of Na_2O_2 and NaO_2 on TiC and found similar trends to that of Li_2O_2 adsorption. Yang et al.[15,16] analyzed the adsorption of Li_xO_2 (x = 1, 2 and 4) molecules on 3d TMC surfaces and found the correlations between ORR overpotentials and the adsorption energies of Li, LiO_2 and surface energies of 3d TMC surfaces.

An important question by itself, is the surface oxidation processes and the formation of oxide layers at the TMCs surface. This question is also relevant to Li_2O_2 adsorption as the Li_2O_2 molecules can adsorb on either a clean or an oxidized surface.

Here, we use density functional theory (DFT) to explore the trends in the adsorption of oxygen and nLi_2O_2 ($n = 1-4$) molecules on TMC surfaces, which comprise 3d, 4d and 5d TM, specifically TM = Ti, V, Zr, Nb, Mo, Hf, Ta. We show the binding of oxygen atoms and then the adsorption of Li_2O_2 molecules on the clean and oxidized TMC surfaces. We show trends in the oxygen binding on the TMC surfaces and compare our results with the experimental findings. We also demonstrate the main trends in structural and adsorption energy properties of the Li_2O_2 molecules on the pristine TMC surfaces and examined the role of the oxygen layer on the adsorption of Li_2O_2 molecules.

Theoretical Approach and Computational Details

We performed total energy calculations of the systems applying Density Functional Theory (DFT) within the recently proposed strongly constrained and appropriately normed (SCAN) semilocal meta-GGA density functional.[17] SCAN was found to have a good prediction of energies and structures for covalent, metallic, ionic, hydrogen, and van der Waals bonds with the accuracy of hybrid functionals, but it is a significantly less costly method.[18] For comparison, we also calculated the total energy and structural parameters of the TMC bulks and pristine and oxydized TMC surfaces with the GGA-PBE[19,20] functional.

We employed the projected augmented wave method (PAW)[21,22] for the DFT calculations, as implemented in the Vienna Ab-initio Simulations Package (VASP).[23,24] We applied a Monkhorst-Pack **k**-point sampling scheme[25] with **k**-point meshes of $10 \times 10 \times 10$, $5 \times 5 \times 1$ and gamma points for the bulk, surface and gas-phase molecules, respectively, and a cutoff energy of 500 eV for all the calculations, except for the bulk calculations, for which we increased cutoff by 2 for the stress tensor minimization procedure. The structural energy minimization procedure was stopped when the atomic forces per atom were smaller than 0.02 eV per Å and a total energy convergence of 10^{-6} eV was achieved.

We calculated the total energy and relaxed structural parameters for the bulk of the 7 TMCs (TM = Ti, V, Zr, Nb, Mo, Hf, Ta), and the Li_2O_2 crystal using initial values from the ICSD database[26] and built from them the surface models with the AFLOW package.[27,28] We applied the repeated geometry slab model in order to built the (111) surfaces for fcc TMC surfaces, while for the MoC system we also created (001)

surface for the hcp MoC and Mo_2C phases. For every fcc system and hcp MoC we employed a 2×2 surface unit cell, 8 layers, and a 21 Å vacuum region between the slabs, which we found enough to prevent interactions between neighboring slab replicas. For the hcp Mo_2C we employed 3 layers (12 atoms) in the slab.

We calculated the surface energy (γ) as

$$\gamma = (E_{slab} - NE_{bulk})/2A_u \ . \quad (1)$$

Here E_{slab} and E_{bulk} are the total energies of the slab and the total energies per atom of the bulk, respectively, N is the number of atoms in the surface slab , and A_u is the area of surface unit cell.

Applying geometrical lattice match algorithm,[29] we found that (0001) Li_2O_2 surface with 1×1 unit cell matches well with the 2×2 unit cell of TMC surfaces. Depending on the TMC surface area, the Li_2O_2(0001) crystal can be compressed or expanded on the TMC surfaces, which can be determined by misfit factor (η, in %) suggested in[12] and area ratio (α).

$$\eta = (1 - \frac{2A_u}{A_u + A}) * 100\% \ , \quad (2)$$

$$\alpha = \frac{A}{A_u} \ , \quad (3)$$

where A is the surface area of the Li_2O_2(001) surface unit cell.

Results

TMC bulks and surfaces and molecule in gas-phase

Most of the TMC bulks are crystallized in a face centered cubic lattice with a rock salt structure, similar to the NaCl crystal. In the case of MoC, multiple phases can be synthesized, for example, by heating amine-metal oxide hybrid at 750^0 C fcc β-MoC is produced, while by heating at 850^0 hcp α-MoC and Mo_2C are formed.[30] Also the choice of hydrocarbons affect the MoC phase formation, for example, utilizing the mixture of hydrogen and methane, as a source of carbon, leads to the MoC hcp structure formation, while the mixture of hydrogen and butane results in the fcc MoC phase.[31] In order to obtain more understanding of the role of MoC phase on the adsorption properties of the molecules, we used here the fcc phase of MoC and hcp phases of MoC and Mo_2C. The Li_2O_2 bulk has a hexagonal lattice structure with the $P63/mmc$ space group.

We present the equilibrium lattice constants a (and c) calculated by us using PBE and SCAN along with literature theoretical[27,28] and experimental[32–37] values in the supporting information (SI). Our PBE results for the a and c values are in a good agreement with the PBE results in the AFLOWLIB project.[27,28] We found that SCAN yields shorter lattice constants compared with the PBE results (by up to 1% for TMC and 2% for Li_2O_2). These shorter a and c are closer to experimental data for all the cases, except for VC, HfC, Mo_2C and Li_2O_2, for which PBE provides better agreement with experimental results. In this work we used the SCAN results of lattice parameters for the further modeling of the slabs.

Table 1 presents surface properties of the systems, such as the surface area (A in Å^2); the surface energy for the TM-terminated surfaces (γ, in meV/Å^2), the surface energy for the TM-terminated surfaces relative to the C-terminated surfaces ($\Delta\gamma$ in meV/Å^2); the work function (Φ in eV); the misfit factor (η, in %) and area ratio (α).

We obtained a clear trend for the surface energies for the TM-terminated surfaces (γ). According to this trend, γ decreases with the occupation of the d-bands, which is consistent with the surface areas of the systems. We also found that the TM-terminated TMC surfaces are more stable than the C-terminated surfaces, that is, $\Delta\gamma$ is negative in all the cases. This is supported by previous results.[38] We found that $\Delta\gamma$ correlates with the occupation of the d bands of the TMC. As the TM-termination is more stable than the C surface termination for TMC surfaces, we use them for further simulations of the surfaces.

We obtained that the area, A, of Li_2O_2(001) (33.223 Å^2), has a larger value than that of the matching surface cells of TiC(111), VC(111),

and MoC surfaces. This leads to the compression ($\eta > 0$, $\alpha > 1$) of $Li_2O_2(0001)$ on these surfaces, while on the remaining surfaces, expansion ($\eta < 0$, $\alpha < 1$) of $Li_2O_2(001)$ occurs. We found that both η and α increase in their absolute values with the occupation of the d bands.

We discussed the lowest energy structure of the gas-phase Li_2O_2 molecule in a previous work.[13] We obtained that the lowest energy structure is the planar rhombus, in which two O and two Li atoms are at opposite corners and Li−O and O−O bond lengths of 1.74 Å and 1.59 Å, respectively. We used this structure as an initial guess for the molecular dynamics simulations on the TMC(111) and MoC surfaces.

Oxygen binding at TMCs surfaces

To investigate the binding energy trends of O_2 molecules at full coverage on the TMC surfaces, we calculated the binding energy per O_2 molecule as:

$$E_b^{O_2} = (E_{tot}^{4O/TMC} - 2E_{tot}^{O_2} - E_{tot}^{TMC})/2 \ , \quad (4)$$

where $E_{tot}^{4O/TMC}$, $E_{tot}^{O_2}$, and E_{tot}^{TMC} are the total energy of TMC-O, pristine TMC and the O_2 molecule in gas-phase.

The possible binding sites for O atoms on the TMC surfaces are top (T), bridge (B), and hollow hcp (H_C) and hollow fcc (H_{TM}) on the TM-terminated TMC surfaces (Figure 1). We found that the O atoms prefer binding on the H_{TM} sites on the TMC(111) surfaces and H_C sites on α-MoC(001) and Mo_2C, which corresponds to the ABC and AB stacking, respectively (Figure 2). As in this work we are interested in the role of O layer on the TMC on the adsorption properties of the molecules, we simulated full coverage of O atoms on the surfaces (ML = 4/4).

We found that O atoms binding to the TMC surfaces is strong and the calculated binding energy $E_b^{O_2}$ is in the range from −6.65 to −11.74 eV (PBE result), while SCAN yields stronger binding, by 3 − 10%. We obtained a clear trend for $E_b^{O_2}$, which becomes smaller with the increase of TM d-band occupation for (111) surfaces, i.e. $E_b^{O_2}(TiC) > E_b^{O_2}(VC)$, $E_b^{O_2}(ZrC) > E_b^{O_2}(NbC) > E_b^{O_2}(MoC)$, and $E_b^{O_2}(HfC) > E_b^{O_2}(TaC)$. The $E_b^{O_2}$ of oxygen molecules on the α-MoC(001) and $Mo_2C(001)$ surfaces are −8.29 eV and −8.42 eV, which is larger than that of the β-MoC(111) surface (−6.35 eV), however still within the $E_b^{O_2}$ trend, i.e. $E_b^{O_2}(ZrC) > E_b^{O_2}(NbC) > E_b^{O_2}(MoC)$. The oxygen binding energy also increases when going down in the periodic table column. Those trends also correlate with the O−TM perpendicular distance.

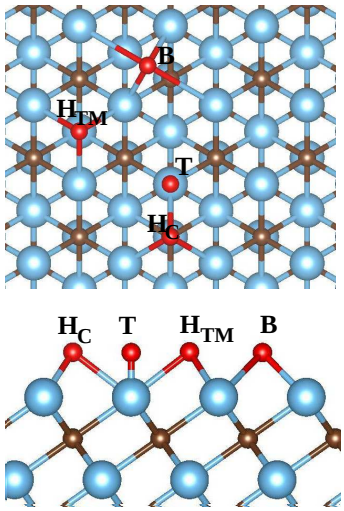

Figure 1: Possible oxygen atoms binding sites on the TMC surfaces.

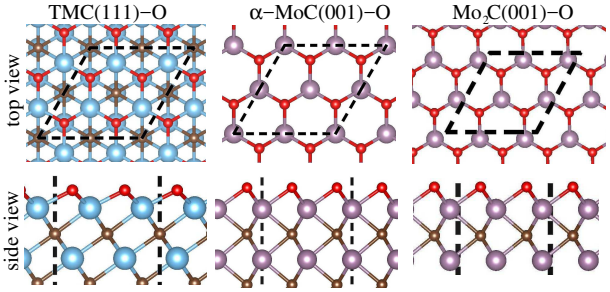

Figure 2: Lowest energy binding sites of O atoms on the TMC(111), α-MoC(001) and $Mo_2C(001)$ surfaces.

In Figure 4 we check the correlation between the experimentally measured oxidation potential of several TMCs, as reported by Kimmel et al.,[39] and our SCAN functional calculated binding energy, $E_b^{O_2}$. While the correlation is not perfect, it is evident that a lower $|E_b^{O_2}|$ correlates with a lower oxidation potential.

Table 1: Surface properties of the TiC(111), VC(111), ZrC(111), NbC(111), β-MoC(111), α-MoC(001), Mo_2C, HfC(111) and TaC(111) surfaces, such as surface area (A, in Å^2), surface energies for TM-terminated surfaces (γ, in meV/Å^2), surface energies for TM-terminated surfaces relative to C-terminated surface ($\Delta\gamma$, in meV/Å^2), work function (Φ, in eV), misfit factor (η, in %), and area ratio (α), obtained by SCAN. The surface area of Li_2O_2(001) is 33.223 Å^2.

	TiC	VC	ZrC	NbC	β-MoC	α-MoC	Mo_2C	HfC	TaC
A	32.40	29.68	38.35	34.63	32.84	29.26	28.11	36.85	34.25
γ	366	306	318	291	211	355	57	352	297
$\Delta\gamma$	−398	−405	−712	−790	−824	−935	−672	−1598	−1748
Φ	4.58	4.44	4.46	4.40	4.72	4.68	4.59	4.84	4.72
η	1.25	5.63	−7.16	−2.07	0.58	6.34	8.34	−5.18	−1.52
α	1.03	1.12	0.87	0.96	1.01	1.14	1.18	0.90	0.97

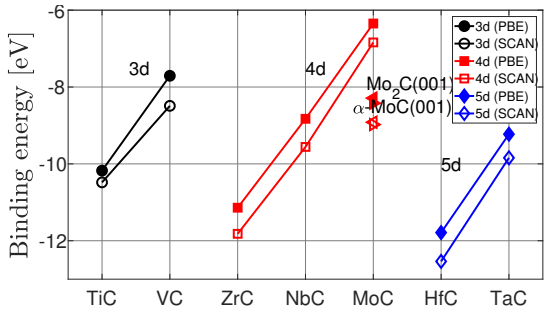

Figure 3: Binding energy of O_2 molecules on the TMC(111), α-MoC(001) and Mo_2C(001) surfaces. The α-MoC(001) and Mo_2C(001) values are almost the same for both PBE and SCAN. Full symbols show the PBE results while empty symbols show the SCAN results.

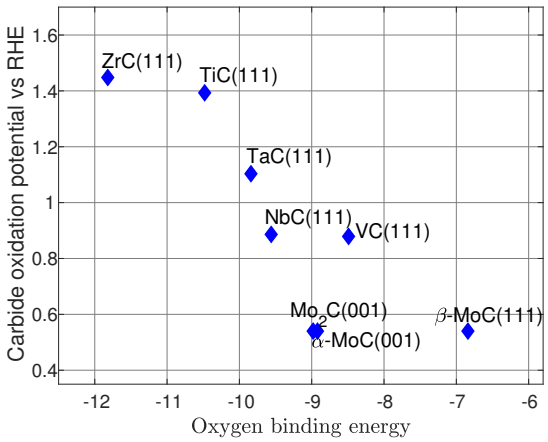

Figure 4: Carbide oxidation porential (taken from Kimmel et al.[39]) vs. the binding energy of O_2 molecules on the TMC(111), α-MoC(001) and Mo_2C(001) surfaces.

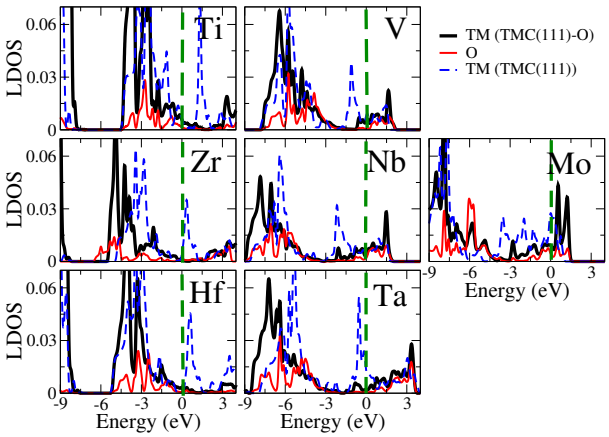

Figure 5: Projected DOS of the pristine (TM states are shown with a dashed blue line) and oxydized (TM states are shown with a solid black line, oxygen states are shown with a solid red line) TMC surfaces. Vertical (green) line corresponds to the Fermi level.

The electronic structure of the pristine and oxidized TMC(111) surfaces can provide additional information on the potential of the molecular adsorption and explain some of the main trends. A detailed analysis of the density of states (DOS) of the TMC bulks and (111) surfaces can be found elsewhere.[38,40] Here we focus on the main characteristics of the atom resolved local density of states (LDOS) of the pristine and oxidized TMC(111) surfaces. Figure 5 presents the LDOS averaged on the surface layers of TMC and O atoms. The following features are found:

(i) states from −30 eV to about −10 eV consist of the C and TM peaks derived from C *s*-states and TM *s*-, *p*- and *d*-states; states from −10 eV to Fermi level are characterized by C and TM peaks, in which C *p*-states and TM *d* states dominate, and states above Fermi level present mostly TM *d* states;

(ii) overall, there is a shift of the TMC states away from Fermi level due to the interaction with the adsorbed oxygen atoms. Moreover, the peaks derived mostly from TM *d* states around the Fermi level disappear upon oxygen adsorption, which implies the loss of reactivity on the oxidized surface;

(iii) hybridization of the O *p*-states with the TMC *d* states, which implies the strong interaction of O layer with the surfaces;

(iv) overall, there is a shift of the TMC states away from Fermi level within a period, with the occupation of TM *d* states, from Ti to V, from Zr to Nb to Mo and from Hf to Ta, which correlates with the binding energy of O on these surfaces.

Li_2O_2 adsorption on the TMC surfaces

Modelling of Li_2O_2 adsorption on carbides

We built the initial models for the adsorbed $n$$Li_2O_2$ molecules on the TMC and TMC-O surfaces with the following procedure:

(i) We placed the Li_2O_2 molecule(s) about 5 Å above the TMC and TMC-O surfaces and applied first-principles molecular dynamics simulations with temperatures from 300 K to 0 K for 30 ps by employing the Nosé thermostat. Then, we optimized the final structures with the conjugated gradient algorithm as implemented in the VASP code.

(ii) After the MD simulation, in most of the TMC-O systems, we found highly distorted molecular and surface layers. In order to cover more possibilities in finding the lowest energy strutures we employed a cross-check procedure in the following way - We took the molecular and surface layers of every lowest energy structure obtained in (i) and exchanged them between the TMCs.

We put the molecules on one side of the slab and allowed the molecules to move along with 6 surface layers. For all the total energy calculations we employed a dipole correction. We performed full geometrical relaxation for all the structures. Finally, we collected the structures and selected the lowest energy configurations for further analysis.

The lowest energy structures of $n$$Li_2O_2$ (n = 1−4) on the pristine and oxidized TMC(111) surfaces are presented in Figures 6, 8 and 9; their structural parameters, such as average perpendicular distances between TM−C and TM−O (in Å), are given in Figure 7; their adsorption energies (E_{ad1} and E_{ad2}) are in Figures 10 and 11.

Li_2O_2 adsorption on pristine TMC surfaces

In the lowest energy configurations the Li_2O_2 molecules form O and Li layers on the TM-C surfaces due to a break of the Li−O bonds and stronger binding to the reactive TM surface atoms. At that, the O atoms bind to the reactive TM-terminated TMC surfaces on the hollow fcc positions, adopting the positions of the missing C atoms, and Li atoms are arranged above the O atoms at the hcp positions of the missing TM atoms, which correspond to the *ABC* stacking of the TMC. The 2 Li_2O_2 adsorbed molecules on the TMC surfaces form a full coverage of O and Li atomic layers. This finding agrees with previous results obtained

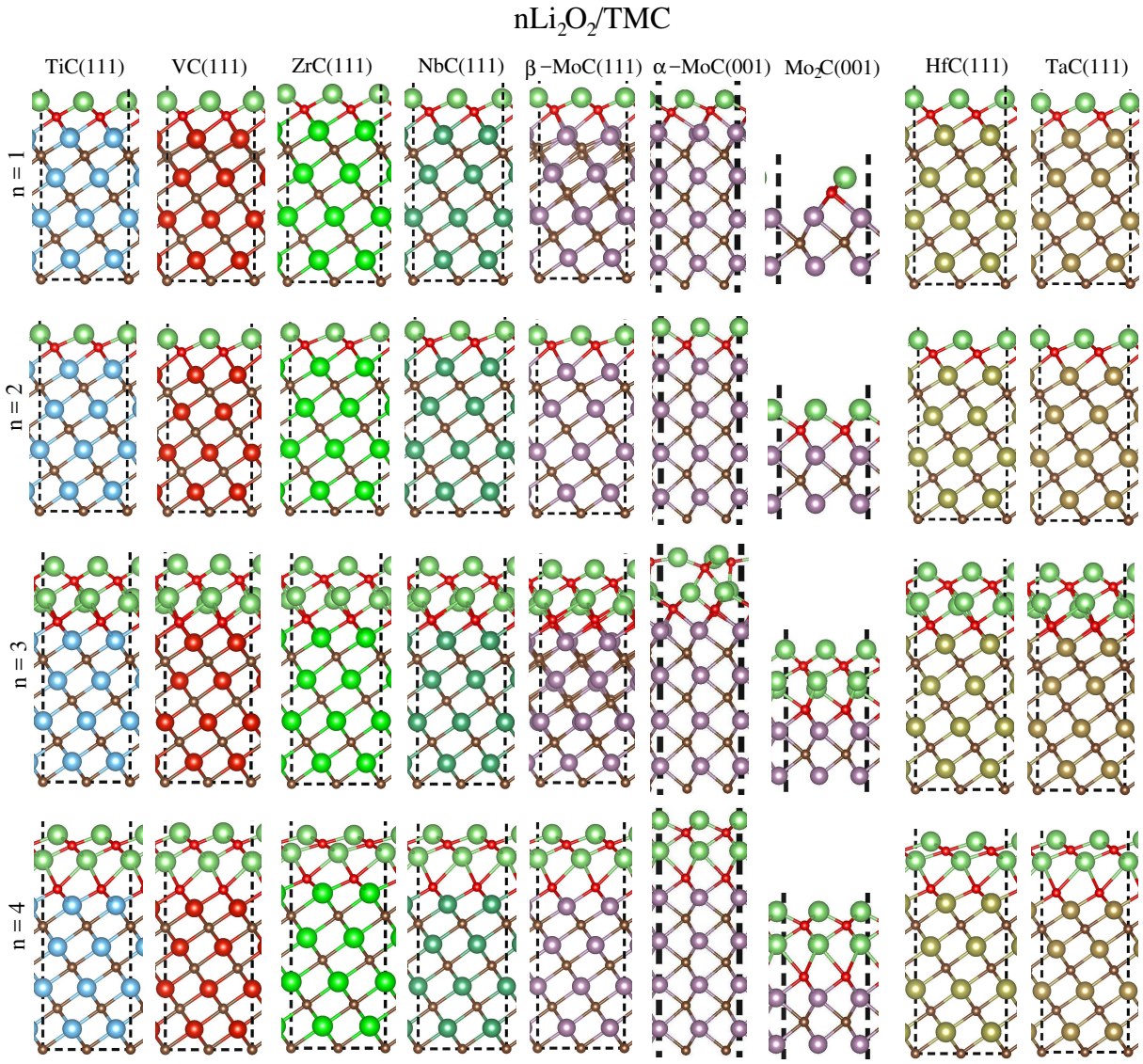

Figure 6: The lowest energy structures of $n\mathrm{Li_2O_2}$ $(n = 1 - 4)$ on the TMC surfaces.

in[12,13] for the adsorption of Li_2O_2 molecules on TiC(111) surface.

At larger molecular density, $n = 3$ and 4, we found that molecules proceed assembling into O/Li/O/Li molecular layers on the TMC surfaces, however, with slight displacement of O and Li atoms from their ideal atomic hcp and fcc hollow positions, as well as in z direction. These structural changes at the second O/Li bilayer can be explained by the beginning of the formation of the native Li_2O_2 crystal structure.

Meanwhile, O and Li layers above the TMC surfaces affect the atomic positions of TM layers in z direction. In order to characterize this phenomenon, we measured the averaged perpendicular TM−C and TM−O distances of systems upon the molecular adsorption and compared them with the pristine and oxidized surfaces (Figure 7). We also calculated a ratio (r) of TM−C and TM−O perpendicular distances between the $n Li_2O_2$/TMC(111) and TMC(111). If $r > 1$ ($r < 1$), there is an expansion (compression) of the layer, which occurs in order to release the strain and reach structural relaxations due to the tensile (compressive) strain arised from above atomic layers.

We found that the TM−C bilayer expands with every subsequent molecular layer, that is, the first two molecules adsorption leads to TM−C expansion by factor $r = 0.98 - 1.07$, while at the adsorption of the next two molecules the layers expand more, i.e. $r = 1.04 - 1.22$, which can be explained by the additional stress caused by addition of the next moleculer layer.

Moreover, the O layers directly bound to the TM atoms and second O layers in the surface Li/O bilayers also expand. For example, we found the larger expansion at $n = 1$,2 ($r = 1.28-1.58$), and smaller one with the formation of the next O/Li layers, from $n = 3$ ($r = 1.15-1.32$) to $n = 4$ ($r = 0.97-1.06$), which implies the Li_2O_2 crystal formation, that is, they are close to the magnitude of Li_2O_2 crystal. For example, for 4 Li_2O_2 on TiC(111) the Li−O perpendicular distances for inner layers are 1.77 Å and for the surface layers there is a compression with the distances of 0.65 Å, while for Li_2O_2 crystal the distances are 1.12 Å and 0.35 Å, respectively.

Thus, initially adsorbed Li_2O_2 molecules form O/Li layers on the TMC surfaces, which retain the atomic positions dictated by the TMC crystal, and subsequent growth of the O/Li layers over TMC surfaces leads to the formation of the native Li_2O_2 crystal structure. However, the adsorption of the 4 molecules is still not enough in order to observe the Li_2O_2 crystal structure and more layers are required to achieve it.

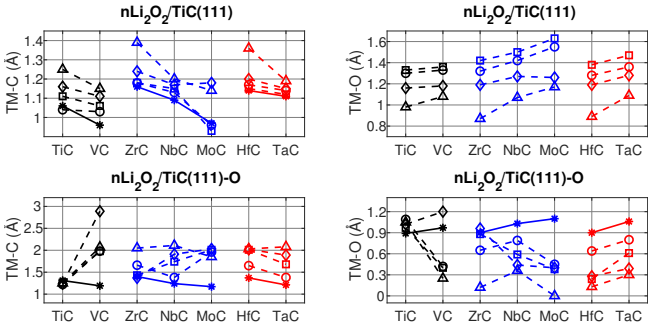

Figure 7: Averaged perpendicular TM−C and TM−O distances in the surface TMC layers upon the $n Li_2O_2$ molecules adsorption. Here ∘, □, ◇ and △ with the dashed lines correspond to 1, 2, 3 and 4 Li_2O_2 molecules on the TMC(111), respectively, and solid lines present the TMC(111) and TMC(111)-O surfaces.

Li_2O_2 adsorption on the oxidized TMC(111) surfaces

The presence of the O layer on the TMC surfaces has a passivation effect, which implies no direct binding of the Li_2O_2 molecules with the reactive TM surfaces. Still a similar behavior appears for the Li_2O_2 adsorption. That is, a break of the Li_2O_2 molecular bonds and a formation of the Li/O layers over the O layer of the surfaces. The presence of the additional O layer between the molecules and the TMC surfaces leads to two scenarios of the structural formation, depending on the TMC surface, which as highly distorted Li/O layers and TM/C surface layers and less distorted retaining the positions of the TMC crystal.

As demonstrated above, O and Li layers on the TMC surfaces induces the expansion of the TM and O layers. It is important to note that

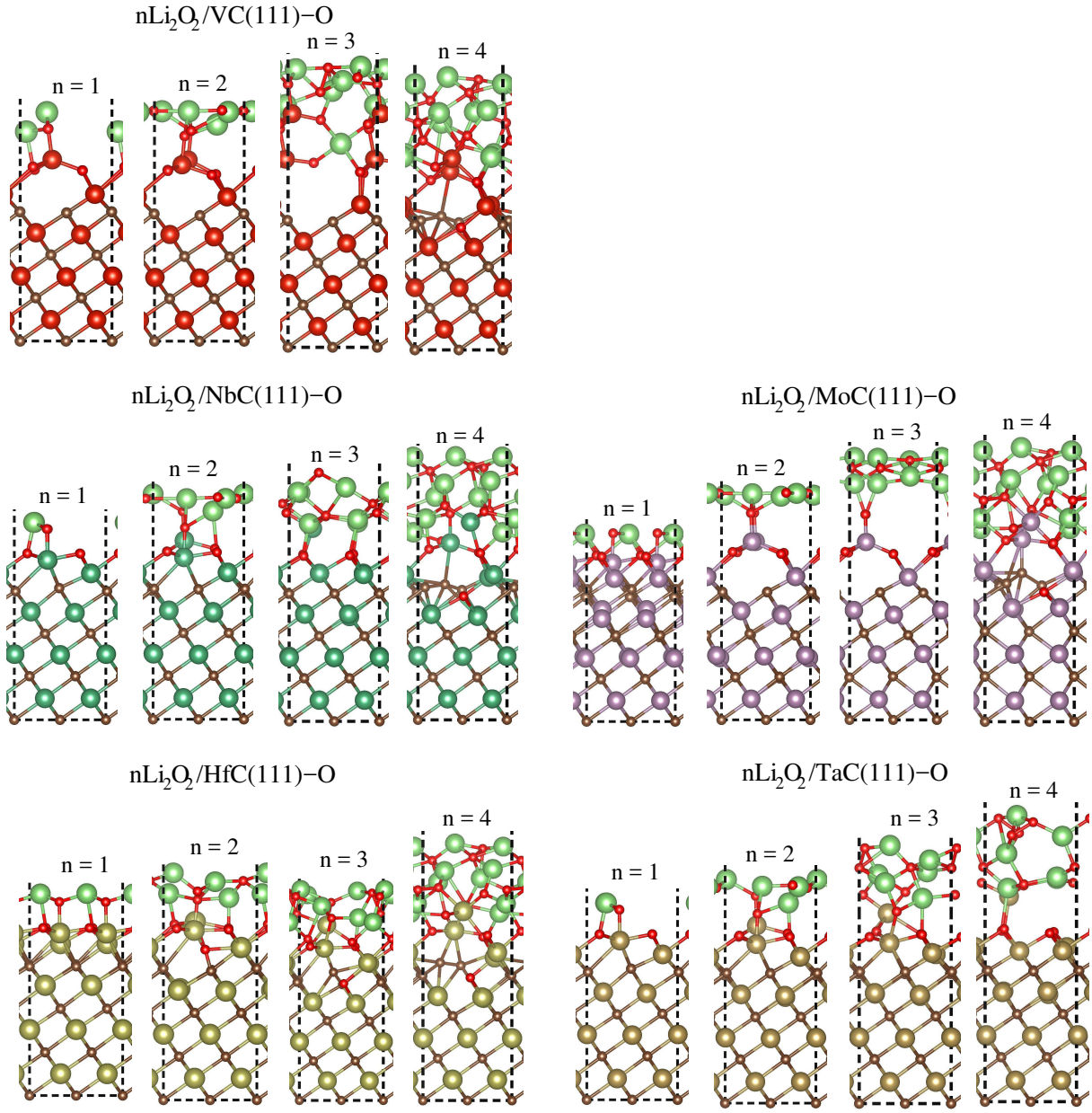

Figure 8: The lowest energy structures of $n\mathrm{Li_2O_2}$ ($n = 1-4$) on the oxidized VC(111), NbC(111), MoC(111), HfC(111) and TaC(111) surfaces.

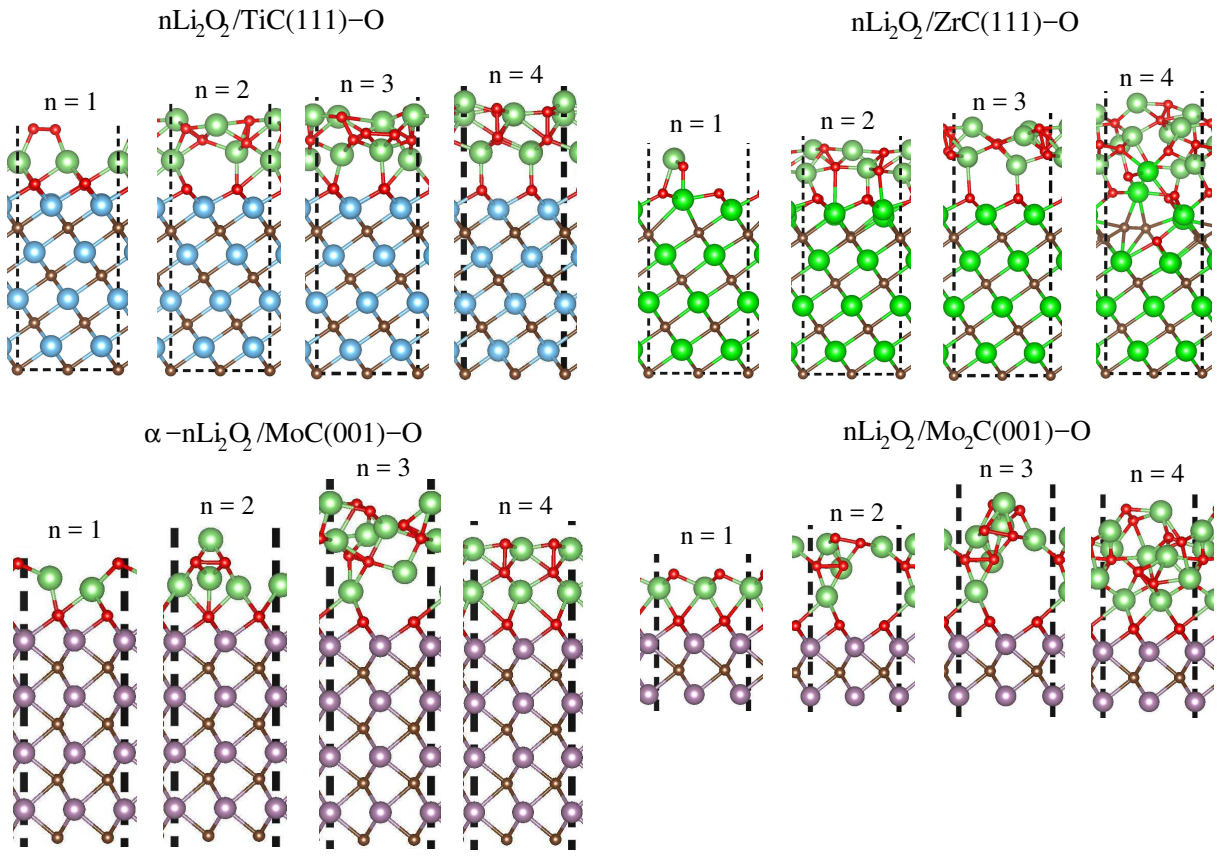

Figure 9: The lowest energy structures of $n\mathrm{Li_2O_2}$ ($n = 1-4$) on the oxidized TiC(111), ZrC(111), α-MoC(001) and $\mathrm{Mo_2C}$(001) surfaces.

the O layer itself (without the molecules) causes a small expansion of the TM layer, by $r = 1.17-1.40$, due to the tensile strain caused by O atoms. When the Li_2O_2 molecules adsorb above the O layer, strain increases more, which leads to larger distortions of individual TM, O and even Li atoms in some systems. For example, the expansion of individual TM atoms increases up to $r = 1.74$ for the VC(111), Nb(111), Hf(111), Ta(111).

Besides, noticeable structural distortions of TM, O and Li atoms in the interface between the Li_2O_2 molecules and TMC(111) (TM = V, Nb, Hf, Ta) surfaces can be explained as the following. The addition of O atoms between the Li_2O_2 and TMC(111) systems may imply the new stoichiometry of Li-oxide, which is above the TMC surfaces, that is the interaction between Li_2O_2 and $2\,O_2$ creates Li_2O_6, which is more stable in a metal lithium oxide compound, i.e. $2\,LiO_3TM_1$.

Such metal lithium oxide formations with the stoichiometry $Li_1O_3TM_1$ for the particular systems of TM = V, Nb, Ta was also found experimentally.[41–43] In the case of β-MoC(111), large structural distortions are found, however it can be also explained by the unstable β-MoC(111) surface at room temperature.

Furthermore, this $Li_1O_3TM_1$ layer formed on the TMC(111) surfaces can be considered as a protective layer, which eliminates further TMC surface degradation at the Li_2O_2 crystal formation.

For the remaining systems, such as the oxidized TiC(111), ZrC(111), α-MoC(001) and Mo_2C(001) surfaces, except for some cases, there are no observable TM and O atomic distortions, rather a small expansion and even compression for TM and O atoms, while Li_2O_2 molecules are adsorbed above. This can indicate that in this systems the O layer functions as a passivation layer in the interface between the Li_2O_2 molecules and the TMCs surfaces. This is in an agreement with literature finding,[8] reported on the creation of the protective TiO_2 layer on the surface, which can also play a role of a reasonable electron transport.

Thus, the presence of the additional O layer in the interface between the nLi_2O_2 molecules and TMC surfaces leads to the change in the stoichiometry of Li-oxide. This results in the formation of the protective $Li_1O_3TM_1$ layer on the VC(111), NbC(111) and TaC(111) surfaces, and the passivation oxygen layer on the TiC(111), ZrC(111) and MoC(001) surfaces. These layers may prevent the surfaces from further degradation upon the adsorption of Li_2O_2 molecules, which allow the Li_2O_2 crystal growth above.

Trends in adsorption energies of Li_2O_2 on the TMC surfaces

We calculated the average adsorption energy per Li_2O_2 molecule on the TMC(111) surfaces as

$$E^n_{ad1} = (E^{\mathrm{n^*mol/TMC}}_{tot} - nE^{\mathrm{molecule}}_{tot} - E^{\mathrm{TMC}}_{tot})/n\ , \tag{5}$$

where n is the number of molecules in the system and $E^{\mathrm{n^*mol/TMC}}_{tot}$, $E^{\mathrm{molecule}}_{tot}$ and E^{TMC}_{tot} correspond to the total energies of the lowest energy structures for nLi_2O_2 molecules on the prisine and oxidized TMC, a single gas-phase molecule, and prisine and oxidized TMC surfaces, respectively.

It is also interesting to calculate the adsorption energy of the n^{th} molecule when it adsorbs on a surface that already has on it $n-1$ molecules, this is given by:

$$\begin{aligned} E^n_{ad2} &= E^{\mathrm{n^*mol/TMC}}_{tot} - E^{\mathrm{(n\text{-}1)^*mol/TMC}}_{tot} - E^{\mathrm{molecule}}_{tot} \\ &= nE^n_{ad1} - (n-1)E^{n-1}_{ad1}. \end{aligned} \tag{6}$$

Here E^n_{ad1} and E^{n-1}_{ad1} correspond to the adsorption energies of the n and $n-1$ molecules on the TMC surfaces and we define $E^0_{ad1} = 0$.

Figures 10 and 11 demonstrate the average adsorption energy per molecule (Eq. 5) and the contribution of the last molecule to the adsorption energy (Eq. 6), respectively. We found the largest adsorption energies, E_{ad1}, (Figures 10) at n = 1,2 of nLi_2O_2 on the TMC(111), which implies the strong binding of the molecules with the reactive TM atoms. The main contribution to E_{ad1} comes from the binding of O atoms to

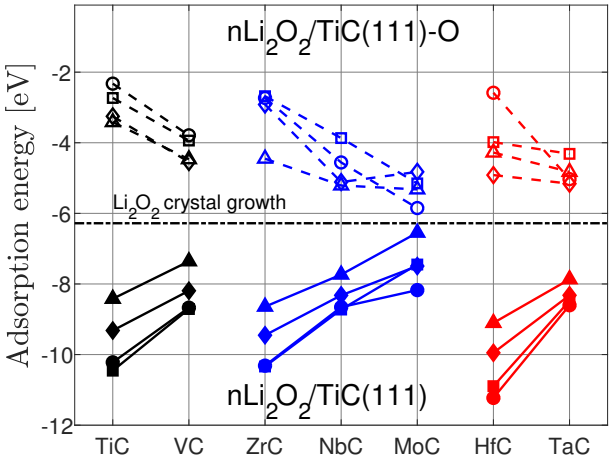

Figure 10: Adsorption energy (Eq. 1) of $n\mathrm{Li_2O_2}$ on pristine and oxidized TMC surfaces. Here $\circ$, $\square$, $\diamond$ and $\triangle$ correspond to 1, 2, 3 and 4 $\mathrm{Li_2O_2}$ molecules, respectively.

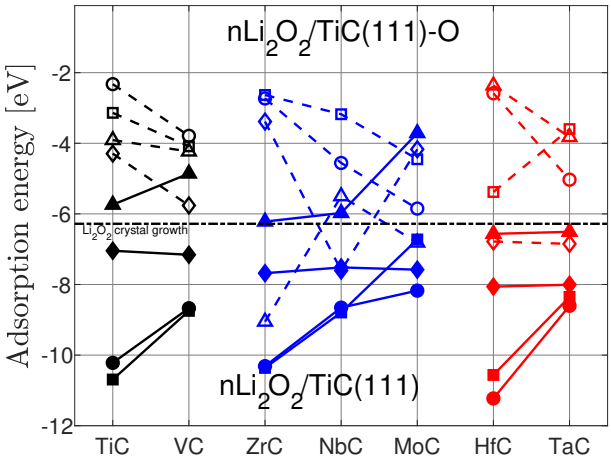

Figure 11: Adsorption energy (Eq. 2) of $n\mathrm{Li_2O_2}$ on pristine (full symbols) and oxidized (empty symbols) TMC surfaces. Here $\circ$, $\square$, $\diamond$ and $\triangle$ correspond to 1, 2, 3 and 4 $\mathrm{Li_2O_2}$ molecules, respectively.

TM atoms, as E_{ad1} (in the range from -8.17 to $-11.23\ eV$) is close to the binding energy of O layer, i.e. $E_b^{\mathrm{O_2}}$. It is also evident that the same trend is observed for the oxygen binding and the $\mathrm{Li_2O_2}$ adsorption at the clean surfaces, that is – the clean TMC surface is less reactive with a higher d-occupation of the metal.

An addition of the third and fourth $\mathrm{Li_2O_2}$ molecules to the TMC surfaces leads to reducing E_{ad1}, as they form the next O and Li layers above the previous Li/O layers. This is can be also seen from Figure 11, that is E_{ad2} is larger for n = 1,2 and decreases for n = 3 and 4.

At the adsorption of the $n\mathrm{Li_2O_2}$ molecules on the oxidized TMC surfaces, the trend is different. The magnitude of the E_{ad1} adsorption energy is up to 4−5 times smaller for 1 and 2 molecules and slightly increases at larger molecular size. At some point E_{ad1} tends to reach some constant value, close to the value for the $\mathrm{Li_2O_2}$ crystal growth.

We also found that E_{ad1} on the pristine carbide surfaces decreases with the occupation of d-band, e.g. from TiC to VC, from ZrC to MoC, and from HfC to TaC. This trend is opposite on the oxidized TMC surfaces, thus implying that with the occupation of the d-bands there is a faster formation of the $\mathrm{Li_2O_2}$ crystal, so that the type of surface and its oxidation state become less important for the $\mathrm{Li_2O_2}$ crystal formation above them.

The values of E_{ad1} for the $\mathrm{Li_2O_2}$ molecules on the α-MoC(001) and $\mathrm{Mo_2C}$(001) surfaces are ranging within the general trend and lying around β-MoC(111) results, i.e. for pristine surfaces from -6.92 to -7.82 eV for $\mathrm{Mo_2C}$(001) and from -7.06 to -8.17 eV for α-MoC(001), while for oxidized surfaces from -1.71 to -3.12 eV for $\mathrm{Mo_2C}$(001) and from -2.89 to -3.21 for α-MoC(001).

Summary and Discussion

We performed DFT calculations and analysis of the adsorption of $\mathrm{O_2}$ and $\mathrm{Li_2O_2}$ molecules on a number of TMC surfaces, containing $3d$, $4d$ and $5d$ elements in order to investigate the main trends in structural and adsorption energy

properties.

We found good qualitative correlation between the oxygen adsorption energy (full monolayer) to the experimentally measured oxidation potential for the different TMCs surfaces.

We demonstrated that the initially adsorbed Li_2O_2 molecules form O and Li layers on the TMC surfaces, retaining the atomic positions determined by the TMC crystals. The O and Li layers induces the tensile strain on the TMC surface atoms, which leads to the expansion of the TM and O layers. The expansion increases when O layer is added to the TMC(111) surfaces. This also leads to the change in stoichiometry of Li-oxide, and hence, to the formation of the protective $Li_1O_3TM_1$ layer on the VC(111), NbC(111), MoC(111), HfC(111) and TaC(111) surfaces which prevent the surfaces from further degradation. For the TiC(111), ZrC(111), α-MoC(001) and Mo_2C(001) surfaces the passivation O layer remains. Above these passivation layer the Li_2O_2 crystal is formed.

We showed that with more than one Li/O molecular bilayer on the TMC surfaces, adsorption energies of the molecules strives to approach their native crystal values.

The adsorption energies of the first Li_2O_2 molecules at the TMCs surface show an opposite trend for the clean and the oxygen passivated cases. For example, the first Li_2O_2 molecule binds stronger to the clean TiC surface than to the clean VC surface, but the opposite is true for the oxygen passivated case. Hence, it would be interesting to compare experimental parameters of the TMC surfaces behavior in the presence of Li_2O_2 to the calculated adsorption energies of Li_2O_2 at both the clean and the more realistic oxygen passivated surfaces.

Acknowledgement This work was supported by the Planing & Budgeting Committee of the Council of High Education and the Prime Minister Office of Israel, in the framework of the INREP project. D. Golodnitsky also thanks the BSF and I-SAEF Foundations for providing financial support (grants BSF 2010174 and I-SAEF PA1359959), which enabled initiation and continuation of the research on sodium-air batteries.

References

(1) Abraham, K. M.; Jiang, Z. A Polymer Electrolyte-Based Rechargeable Lithium/Oxygen Battery. *J. Electrochem. Soc.* **1996**, *143*, 1–5.

(2) Cheng, F.; Chen, J. Metal-Air Batteries: from Oxygen Reduction Electrochemistry to Cathode Catalysts. *Chem. Soc. Rev.* **2012**, *41*, 2172–2192.

(3) Luntz, A. C.; McCloskey, B. D. Nonaqueous Li-Air Batteries: A Status Report. *Chem. Rev.* **2014**, *114*, 11721–11750.

(4) Ma, Z.; Yuan, X.; Li, L.; Ma, Z.-F.; Wilkinson, D. P.; Zhang, L.; Zhang, J. A Review of Cathode Materials and Structures for Rechargeable Lithium-Air Batteries. *Energy Environ. Sci.* **2015**, *8*, 2144–2198.

(5) Dong, Q.; Wang, D. Catalysts in metal-air batteries. *MRS Communications* **2018**, *8*, 372–386.

(6) Gallant, B. M. Chemical and Morphological Changes of LiO_2 Battery Electrodes Upon Cycling. *J. Phys. Chem. C* **2012**, *116*, 20800–20805.

(7) Thotiyl, M. M. O.; Freunberger, S. A.; Peng, Z.; Chen, Y.; Liu, Z.; Bruce, P. G. A Stable Cathode for the Aprotic Li−O−2 battery. *Nat. Mater.* **2013**, *12*, 1050.

(8) Kozmenkova, A. Y.; Kataev, E. Y.; Belova, A. I.; Amati, M.; Gregoratti, L.; Velasco-Velez, J.; Knop-Gericke, A.; Senkovsky, B.; Vyalikh, D. V.; Itkis, D. M. et al. Tuning Surface Chemistry of TiC Electrodes for Lithium−Air Batteries. *Chem. Mater.* **2016**, *28*, 8248–8255.

(9) Kundu, D.; Black, R.; Adams, B.; Harrison, K.; Zavadil, K.; Nazar, L. F. Nanostructured Metal Carbides for Aprotic Li−O_2 Batteries: New Insights into Interfacial Reactions and Cathode Stability. *J. Phys. Chem. Lett.* **2015**, *6*, 2252–2258.

(10) Faktorovich-Simon, E.; Natan, A.; Peled, E.; Golodnitsky, D. Comparison of the Catalytic Activity of Carbon, Spinel-Based, and Carbide Materials in the Na-Air Battery. *Front. Mater.* **2019**, *6*, 249.

(11) Wang, Z.; Sun, J.; Cheng, Y.; Niu, C. Adsorption and Deposition of Li_2O_2 on TiC111 Surface. *J. Phys. Chem. Lett.* **2014**, *5*, 3919–3923.

(12) Wang, Z.; Chen, X.; Cheng, Y.; Niu, C. Adsorption and Deposition of Li_2O_2 on the Pristine and Oxidized TiC Surface by First-principles Calculation. *J. Phys. Chem. C* **2015**, *119*, 25684–25695.

(13) Raz, K.; Tereshchuk, P.; Golodnitsky, D.; Natan, A. Adsorption of Li_2O_2, Na_2O_2, and NaO_2 on TiC(111) Surface for Metal-Air Rechargeable Batteries: A Theoretical Study. *J. Phys. Chem. C* **2018**, *122*, 16473–16480.

(14) Yang, Y.; Xue, X.; Qin, Y.; Wang, X.; Yao, M.; Qin, Z.; Huang, H. Oxygen Evolution Reaction on Pristine and Oxidized TiC (100) Surface in Li–O2 Battery. *The Journal of Physical Chemistry C* **2018**, *122*, 12665–12672.

(15) Yang, Y.; Qin, Y.; Xue, X.; Wang, X.; Yao, M.; Huang, H. Intrinsic Properties Affecting the Catalytic Activity of 3d Transition-Metal Carbides in Li$-O_2$ Battery. *J. Phys. Chem. C* **2018**, *122*, 17812–17819.

(16) Yang, Y.; Wang, Y.; Yao, M.; Wang, X.; Huang, H. First-principles study of rock-salt early transition-metal carbides as potential catalysts for Li–O 2 batteries. *Physical Chemistry Chemical Physics* **2018**, *20*, 30231–30238.

(17) Sun, J.; Remsing, R. C.; Zhang, Y.; Sun, Z.; Ruzsinszky, A.; Peng, H.; Yang, Z.; Paul, A.; Waghmare, U.; Wu, X. et al. Accurate First-principles Structures and Energies of Diversely Bonded Systems from an Efficient Density Functional. *Nature Chemistry* **2016**, *8*, 831–836.

(18) Sun, J.; Ruzsinszky, A.; Perdew, J. Strongly Constrained and Appropriately Normed Semilocal Density Functional. *Phys. Rev. Lett.* **2015**, *115*, 036402.

(19) Perdew, J. P.; Chevary, J. A.; Vosko, S. H.; Jackson, K. A.; Pederson, M. R.; Singh, D. J.; Fiolhais, C. Atoms, Molecules, Solids, and Surfaces: Applications of the Generalized Gradient Approximation for Exchange and Correlation PW91 Reference. *Phys. Rev. B* **1992**, *46*, 6671–6687.

(20) Perdew, J. P.; Burke, K.; Ernzerhof, M. Generalized Gradient Approximation Made Simple. *Phys. Rev. Lett.* **1996**, *77*, 3865.

(21) Blochl, P. Projector Augmented-Wave Method. *Phys. Rev. B* **1994**, *50*, 17953–17979.

(22) Kresse, G.; Joubert, J. From Ultrasoft Pseudopotentials to the Projector Augmented-Wave Method. *Phys. Rev. B* **1999**, *59*, 1758–1775.

(23) Kresse, G.; Furthmüller, J. Efficient Iterative Schemes for Ab Initio Total-Energy Calculations Using a Plane-Wave Basis Set. *Phys. Rev. B* **1996**, *54*, 11169.

(24) Hafner, J. Ab-initio simulations of materials using VASP: Density-functional theory and beyond. *Journal of Computational Chemistry* **2008**, *29*, 2044–2078.

(25) Monkhorst, H. J.; Pack, J. D. Special Points for Brillouin-Zone Integrations. *Phys. Rev. B* **1976**, *13*, 5188.

(26) ICSD crystallographic database. `https://icsd.fiz-karlsruhe.de/search/basic.xhtml`, Accessed: Jan 2017.

(27) Curtarolo, S.; Setyawan, W.; Hart, G. L. W.; Jahnatek, M.; Chepulskii, R. V.; Taylor, R. H.; Wang, S.; Xue, J.; Yang, K.;

Levy, O. et al. AFLOW: An Automatic Framework for High-Throughput Materials Discovery. *Comput. Mat. Sci.* **2012**, *58*, 218.

(28) Taylor, R. H.; Rose, F.; Toher, C.; Levy, O.; Yang, K.; Nardelli, M. B.; Curtarolo, S. A RESTful API for exchanging materials data in the AFLOWLIB.org consortium. *Comput. Mater. Sci.* **2014**, *93*, 178–192.

(29) Zur, A.; McGill, T. C. Lattice Match: An Application to Heteroepitaxy. *J. Appl. Phys.* **1984**, *55*, 378–386.

(30) Wan, C.; Regmi, Y. N.; Leonard, B. M. Multiple Phases of Molybdenum Carbide as Electrocatalysts for the Hydrogen Evolution Reaction. *Angewandte chemie* **2014**, *126*, 6525–6528.

(31) Xiao, T.; York, A. P. E.; Coleman, K. S.; Claridge, J. B.; Sloan, J.; Charnock-band, J.; Green, M. L. H. Effect of Carburising Agent on the Structure of Molybdenum Carbides. *J. Mater. Chem.* **2001**, *11*, 3094–3098.

(32) Elliott, R. O.; Kempter, C. P. Thermal Expansion of Some Transition Metal Carbides. *J. Phys. Chem.* **1958**, *62*, 630–631.

(33) Nartowski, A. M.; Parkin, I. P.; MacKenzie, M.; Craven, A. J.; MacLeod, I. Solid State Metathesis Routes to Transition Metal Carbides. *J. Mater. Chem.* **1999**, *9*, 1275–1281.

(34) Williams, W. S. Transition Metal Carbides, Nitrides, and Borides for Electronic Applications. *JOM* **1997**, *49*, 38–42.

(35) Guillermet, A. F.; Higlund, J.; Grimvall, G. Cohesive Properties of 4*d*-Transition-Metal Carbides and Nitrides in the NaCl-type Structure. *Phys. Rev. B* **1992**, *45*, 11557–11567.

(36) Yao, K. P. C.; Kwabi, D. G.; Quinlan, R. A.; Mansour, A. N.; Grimaud, A.; Lee, Y.-L.; Lu, Y.-C.; Shao-Horn, Y. Thermal Stability of Li_2O_2 and Li_2O for Li-Air Batteries: In Situ XRD and XPS Studies. *Journal of The Electrochemical Society* **2013**, *160*, A824–A831.

(37) Chrysanthou, A.; Grieveson, P. The observation of metastable molybdenum carbides. *J. Mater. Sci. Lett.* **1991**, *10*, 145–146.

(38) Vojvodic, A.; Ruberto, C.; Lundqvist, B. I. Atomic and Molecular Adsorption on Transition-Metal Carbide (111) Surfaces from Density-Functional Theory: a Trend Study of Surface Electronic Factors. *J. Phys.: Condens. Matter.* **2010**, *22*, 375504.

(39) Kimmel, Y. C.; Xu, X.; Yu, W.; Yang, X.; Chen, J. G. Trends in Electrochemical Stability of Transition Metal Carbides and Their Potential Use As Supports for Low-Cost Electrocatalysts. *ACS Catalysis* **2014**, *4*, 1558–1562.

(40) Vojvodic, A.; Ruberto, C. Trends in Bulk Electron-Structural Features of Rocksalt Early Transition-Metal Carbides. *J. Phys.: Condens. Matter.* **2010**, *22*, 375501.

(41) Muller, C.; Valmalette, J.-C.; Soubeyroux, J.-L.; Bouree, F.; Gavarri, J.-R. Structural Disorder and Ionic Conductivity in $LiVO_3$: A Neutron Powder Diffraction Study from 340 to 890 K. *J. Solid State Chem.* **2001**, *156*, 379–389.

(42) Abrahams, S. K.; Marsh, P. Defect structure dependenceon composition in Lithium Niobate. *Acta Cryst.* **1986**, *B42*, 61–68.

(43) Abrahams, S. C.; Bernstein, J. L. Ferroelectric lithium tantalate - 1. Single crystal X-ray diffraction study at 24 C. *J. Phys. Chem. Solids* **1967**, *28*, 1685–1692.